IEEE Access
Multidisciplinary | Rapid Review | Open Access Journal

Received June 25, 2019, accepted July 1, 2019, date of publication July 5, 2019, date of current version July 25, 2019.

Digital Object Identifier 10.1109/ACCESS.2019.2927054

Recent Advances in the Hardware of Visible Light Communication

YILIN ZHANG[1], LU WANG[1], KAI WANG[3], KAM SING WONG[2], AND KAISHUN WU[1,4]

[1]College of Computer Science and Software Engineering, Shenzhen University, Shenzhen 518060, China
[2]Department of Physics, The Hong Kong University of Science and Technology, Hong Kong 999077
[3]Department of Electrical and Electronic Engineering, Southern University of Science and Technology, Shenzhen 518055, China
[4]PCL Research Center of Networks and Communications, Peng Cheng Laboratory, Shenzhen 518055, China

Corresponding author: Kaishun Wu (wu@szu.edu.cn)

This work was supported in part by the China NSFC under Grant 61872246 and 61872248, in part by the Guangdong NSF under Grant 2017A030312008, in part by Guangdong Special Support Program, in part by the Fok Ying-Tong Education Foundation for Young Teachers in the Higher Education Institutions of China, GDUPS (2015), under Grant 161064, and in part by Shenzhen Science and Technology Foundation under grant JCYJ20170817095418831.

ABSTRACT Visible light communication (VLC) is an emerging technology that can transform lighting facilities into access points for wireless communication. Its development is bottlenecked by the cut-off frequencies (e.g., −6-dB electrical cut-off frequency f_c and −3-dB electrical cut-off frequency $f_{-3\ dB}$) of hardware, such as light-emitting diodes (LEDs), color converters, and photodetectors (PDs). In the past decade, especially in 2018, many materials and devices have been tested for properties related to VLC, such as f_c, response time, and transmission data rates, which are listed and analyzed here to get an updated overall picture. The $f_{-3\ dB}$ for the latest blue LED and color converter can reach up to 1485 and 470 MHz, respectively, which are great improvements from <5 MHz for conventional white LEDs. Among the new PDs, the largest characterized f_c is 4.2 MHz. Moreover, the smallest response time of these PDs is 0.95 ns, which is promising to have f_c of hundreds of megahertz. The limitation in the field of view when the active area is reduced to enlarge f_c of the PD can be partially overcome with novel fluorescent antenna, whose f_c is more than 40 MHz. These increments in the f_c or $f_{-3\ dB}$ of hardware not only enlarge the channel capacity of the VLC but also facilitate the channel impulse response measurement, and the system becomes more susceptible to changes in the environment. These advances will shed light on the future development of the VLC with faster speed, more portable devices, and more applications for the Internet of Things.

INDEX TERMS Optical wireless communication, physical layer, transceiver, micro-LED, aggregation-induced emission, perovskite, quantum dot, channel modeling.

I. INTRODUCTION

As the amount of data transmitted through wireless networks is increasing, visible light communication (VLC) together with millimeter wave (mmWave) are upcoming techniques to complement the less-sufficient radio frequency (RF) communication. VLC is a wireless communication approach that uses visible light emitted from a light source like a light-emitting diode (LED) to convey information through a wireless channel such as air or water. Compared to traditional RF communication, VLC has the following advantages: it has a lower power consumption than RF for short-range links [1] as it can transmit data while lighting; it can avoid unwanted data leakage as the rectilinear propagation of light can be easily blocked. Also, it is suitable for sensitive scenarios like airplanes and hospitals as it has little electromagnetic interference with electrical instruments; it is a promising candidate for underwater communication with its much weaker absorption in water than RF. However, the limited cut-off frequencies of hardware are significant constraints for VLC development. For example, conventional white LEDs limit the cut-off frequencies to ∼5 MHz [2].

To improve the data transmission performance of VLC, most of the previous works in communication society are mainly focused on modifying the modulation and coding schemes, and there are few overviews of the advances in hardware components, especially transmitters and receivers. This work is aimed to provide the latest update in the past decade on the progress in the VLC hardware, i.e., transmitters which consist of LEDs and color converters as well as photodetector (PD) receivers. We will discuss their properties related to communication performance according to the

The associate editor coordinating the review of this manuscript and approving it for publication was Fang Yang.

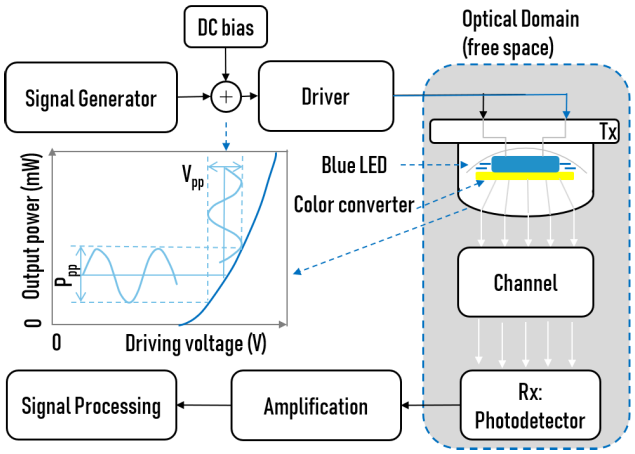

FIGURE 1. Diagram of VLC system architecture using a white LED with color converter. The inset is a relation between the output power and driving voltage for a blue LED chip.

recent published experimental data, as well as their further influence taking the channel into account. Overall, this article is outlined as follows: (1) an introduction to the VLC system architecture; (2) the importance and background knowledge of the cut-off frequency (e.g. −6dB-electrical cut-off frequency f_c and −3dB-electrical cut-off frequency f_{-3dB}) will be introduced and discussed when VLC performance is considered; (3) the recent advances of the hardware in transmitters (LEDs and color converters) and PD receivers will be reviewed; (4) the influence of the hardware improvement on the channel will be discussed.

II. VLC SYSTEM ARCHITECTURE

A diagram of VLC system architecture using a conventional white LED is illustrated in Figure 1. In a typical VLC system, the transmitter (Tx) is a light source with fast on-off switching capability, such as a LED, laser diode (LD) or screen, while the receiver is a PD or camera. Systems using screens and cameras are more complex than the LED and PD combination. To simplify, it is the VLC system that consists of one LED and one PD which is mainly investigated in this work.

During communication, the data are uploaded to the LED transmitter through electric modulation by the signal generator. A direct current (DC) bias is added to the driver via bias-T to offset the driving voltage of the LED to its operating region, according to the relation between the output power and driving voltage in the inset of Figure 1. The electric modulation is converted into an intensity-modulated visible-light signal by the white LED transmitter. After its propagation through the wireless channel, the visible-light signal received by the PD is transformed back into electrical signal and then analyzed by the signal processing part.

A typical white LED consists of a blue LED chip and a layer of color converter on top. The blue LED emits blue light through electroluminescence, and the color converter converts part of the emitted blue light to yellow or orange light through photoluminescence (PL). Then overall white light emission suitable for indoor lighting can be achieved. Recently an emerging flat panel display technology called μLED (also known as micro-LED) has been introduced into the VLC scenario as a new option for the LED chip. The micro-size individual pixel elements of μLED are promising to achieve better communication performance (this will be discussed in Section IV A1)) [3].

The PDs used in VLC are mainly categorized into P-I-N photodiodes (PINs), Schottky barrier photodiodes and avalanche photodiodes (APDs). The PINs lack internal gain, so that an incoming photon can only produce one electron-hole pair before external amplification. In Schottky barrier photodiodes, a thin metal layer replaces either the P-region or N-region of the PINs. The APD provides built-in gain through avalanche multiplication, which can achieve a greater level of sensitivity and higher speed compared to PIN, although it may also require higher operating voltage and have lower reliability. The semiconductor material commonly used as the active layer in PDs of the visible region is silicon (Si). Recently the emerging photovoltaic material called perovskite has also been tested as the active layer in PDs for VLC [4]–[8].

III. BACKGROUND OF CUT-OFF FREQUENCY

When a VLC system is to be built by choosing the suitable hardware, the maximum transmission data rate is one of the major considerations. The upper bound of transmission data rate can be predicted according to the Shannon-Hartley theorem [9], i.e., the channel capacity C is bounded by:

$$C = B \cdot log_2\left(1 + S/N\right) \tag{1}$$

where B is the modulation bandwidth, S is the power of the signal and N is the power of noise. B can be equal to (lowpass case) or smaller than (bandpass case) the f_c, depending on the specific communication scenario. Inspired by the discussion in recent published work [10], [11], the f_c is influenced by the modulation frequency response of the transmitter, receiver, and channel, as shown in Figure 2. $H_b, H_c, H_{ch}, H_p\,(\omega)$ refer to the modulation frequency responses of the blue LED, color converter, channel and PD respectively, α is the fraction of absorption of blue light, η refers to the power ratio between the emitted light and the absorbed light by the color converter (different from the PL quantum efficiency ϕ which refers to the number of photon ratio between the emitted light and absorbed light), R is the PD responsivity, and $P_{b0}, P_b, P_c, P_w, P_f\,(\omega, t)$ refer to the alternating current (AC) signal power of the driving voltage, blue light, color-converted light, white light, and final output of the PD at certain angular frequency $\omega = 2\pi f$ and certain time t.

The proposed response propagation in Figure 2 suggests that the evolution of the modulation frequency response of a VLC system can be estimated by the frequency response of the blue LED, color converter, channel and PD individually. For those whose modulation frequency response exhibits a lowpass feature like color converters, their changes in frequency response can be approximately characterized by changes in f_c. Therefore, a detailed literature search was

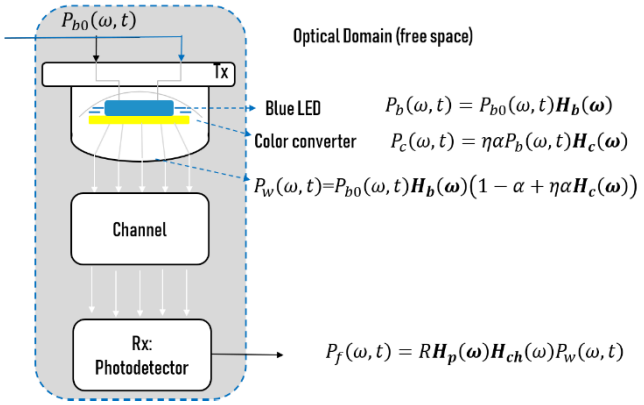

FIGURE 2. Diagram of the modulation frequency response propagation along the optical domain of a VLC system.

performed on the recent published work considering f_c (and sometimes the response time τ_r or carrier lifetime τ related to f_c) of the blue LEDs, color converters and PDs, and the results are listed in Table 1-3.

In this work, it is the f_c rather than signal to noise ratio (SNR) or data rate that is more focused on, and the reasons for this are listed as follows: according to our previous work [12], the signal power S collected by the PD is determined by $S = \int P(\lambda) G(\lambda) R(\lambda) d\lambda$, where $P(\lambda)$ is the optical power distribution of the light emitted from the transmitter, $G(\lambda)$ is the optical collection efficiency of the optical system and $R(\lambda)$ is the response of the PD at wavelength λ [13]. This means that the SNR is susceptible to collection efficiency, such as distance and orientation between the transmitter and receiver, rather than an isolated property of a single hardware part. Furthermore, the dependency of data rate on SNR also makes data rate susceptible to the alignment of the transmitter and receiver. Hence, it is the f_c that is more focused on in the following discussion about the recent advances in the hardware like transmitters or receivers separately.

Also, it should be noted that there are several terms representing the f_c in the recent publications, such as -3dB -optical, -3dB-electrical, -6dB-electrical and electrical-to-optical (E-O) -3dB modulation bandwidths or cut-off frequencies. In this work, without extra notation, the f_c refers to the modulation frequency where the optical modulation amplitude (such as the voltage read from the oscilloscope) reduces to half of the maximum (i.e. -3dB optical, or -6dB electrical), and the $f_{-3\text{dB}}$ refers to the modulation frequency where the optical modulation power (such as the power read from the spectrum analyzer) reduces to half of the maximum (i.e. -3dB electrical). For color converter, their relations with corresponding carrier (PL) lifetime τ are approximately $f_c = \sqrt{3}/(2\pi\tau)$ while $f_{-3dB} = 1/(2\pi\tau)$ [10], [12], [14].

IV. RECENT ADVANCES OF THE HARDWARE

A. TRANSMITTER

1) LED AND μLED

According to the previous works, the conventional semiconductor blue LED had a cut-off frequency of a few to 20 MHz [15]. As listed in Table 1, in the past decades, researchers have proposed several new prototypes of LEDs and μLEDs that can extend the f_c of blue LED to more than 1GHz [10], [16], even higher than the laser diode (Osram PLT5 450B) used as the excitation source for the color converters in some VLC tests [12], [17]. With the spreading use of LEDs in lighting and μLEDs in display applications, these advances can greatly facilitate VLC to achieve the Gbps transmission data rate.

For LED devices, f_c is inversely proportional to the total response time τ_r, and the τ_r includes the resistance- capacitance (RC) time constant τ_{RC} and the τ [10], [18]. Hence trials have been made to improve the f_c of LED devices by reducing the τ_{RC} or τ. Considering $\tau_{RC} = RC$, where R is the resistance, C is the electrical capacitance related to the active area A of the detector; thus, τ_{RC} will decrease with shrinking A. As the typical size of the LED chip for lighting applications is 1 mm $\times$ 1 mm or greater [19], while μ LED features a miniature length less than 100 μm, i.e. only 1% A of LED [20]; thus, replacing the conventional LED with μLED can reduce the C [1], and the corresponding τ_{RC}. However, the effect of reducing τ_r by reducing A has some limits. For example, comparing the f_c of four pixel sizes in Zhu's report [21], i.e. the first three have a mesa diameter = 60, 90, 120 μ m, and the last one has a pixel size of 540 $\times$ 450 μm^2, it can be found that the f_c of these four LEDs are almost the same, suggesting that when the pixel size of these LEDs shrinks down below 540 $\times$ 450 μm^2, it is the τ rather than τ_{RC} that dominates the τ_r. This is also supported by the τ_{RC} of around 0.1 ns and τ of at least 0.263 ns in Cao's recent publication [10].

As the carrier lifetime τ can be expressed by $1/(k_r + k_{nr})$, the way to reduce τ without compromising energy conversion efficiency is to improve the carrier recombination rate k_r. One way to enhance k_r in these semiconductors is to increase the overlap between electron and hole wavefunction in spatial integrals in the active layer of the device via means like tuning lattice strain [22]–[24], or suppressing the quantum confinement stark effect (QCSE) [10], [16], [18], [21], [25], [26].

To tune lattice strain, approaches like photonic crystal [22], nanowire [23], and external strain compensation [24] have been tested, leading to the f_c of 347, 1020 and 117 MHz (-3dB-electrical for [24]). To suppress the QCSE, one approach is to reduce the thickness of the quantum well (QW) [10], [18], [21], [25], [27]. However, reducing the thickness of QW may prolong the τ when the thickness is smaller than a certain value, as the localized carriers become more likely to be trapped inside the potential minima in QWs [21].

Therefore, experimental efforts have been made to optimize the thickness [21]. So far the $f_{-3\text{dB}}$ can go up to 1040 MHz for a 3 nm-thick InGaN multiple quantum well (MQW) on c-axial patterned sapphire substrate [10], and 1485 MHz for a 6 nm-thick nonpolar m-Plane InGaN/GaN MQW on free-standing GaN [16].

It should be noted that the performance of the LED and μLED are also influenced by the detailed LED

TABLE 1. Recent progress in LED and μLED materials.

Year	Ref	Material	Emission peak [nm]	diameter	τ [ns]	f_c [MHz]	Current density of f_c	Modulation scheme	Data rate [Mbps]
LED									
2018	[18]	blue LEDs with ultra-thin InGaN (1 nm)/GaN(3 nm) on c-plane sapphire substrate	440	300 μm	1.41	120[a] 536[a]	56 A/cm^2 2.5 kA/cm^2		
2017	[22]	GaN LED with photonic crystal	~446	20,40,60,80,120 μm	0.46 (20 μm)	347(20 μm) 112(120 μm)	3 kA/cm^2	NRZ-OOK	500 (120 μm)
2017	[21]	GaN LED with 2,3, or 5 nm thick InGaN MQW	440,450, 460	60, 90, 120 μm, and A = 540×450 μm^2	~1 (5 nm thick)	20 700	10 A/cm^2 425 A/cm^2		
2016	[23]	Ultrabroad linewidth orange-emitting InGaN/GaN nanowire (NW) LED	614			1020		NRZ-OOK	1060
2016	[24]	InGaN/GaN LEDs with tuned strain compensation	480 545		1.37 2.14	117[a] (480 nm)			
2014	[15]	Conventional semiconductor blue LED	~450			A few to ~20			
2013	[30]	OLED	604,510, 470	80 mm		0.093		MLP-ANN	2.7
2009	[31]	OLED based on TFB:F8BT	545	A = 0.018 mm^2.	2 (τ_r~30)	26			
μLED									
2019	[10]	Flip-chip GaN with 3 nm thick InGaN MQW on c-axial patterned sapphire substrate	467	30 μm	0.263[b]	1040[a]	20 kA/cm^2	NRZ-OOK	675 (white LED)
2018	[16]	nonpolar m-Plane InGaN (6 nm)/GaN (15 nm) MQW on free standing GaN	454	80 μm	0.2 (τ_{RC}: 0.02~0.05)	1485 [a]	1 kA/cm^2		
2018 2017	[26, 32]	top-emitting (p-up) InGaN/GaN MQW μLED , similar to [25]	445	80 μm		160		NRZ-OOK	300 (with YQD) 800(under water)
2017	[33]	flip-chip GaN violet μLED in circular arrays	405	Inner: A = 435 μm^2 (equivalent to a diameter of 24 μm), Outer: A = 465 μm^2		655	50 mA	QAM-OFDM	11950
2016	[34]	flip-chip μLED in circular arrays with Pd p-contact metal	450	equivalent to inner: 24 μm Outer: 42 μm	0.19	830	16 kA/cm^2	NRZ-OOK	1700
2016	[27]	MQW LED with InGaN (3 nm)/GaN(5 nm)	480	50 μm		960	5 kA/cm^2		
2014	[28]	top-emitting (p-up)InGaN/GaN MQW on Si	470	45 μm		190 270	375 A/cm^2 6875[c] A/cm^2	NRZ-OOK	400
2014	[25]	top-emitting 2.8 nm-thick InGaN/GaN MQW on c-plane sapphire substrate	445	40 μm		60 160	~500 A/cm^2 2800 A/cm^2		
2012	[29]	flip-chip AlInGaN μLED on c-plane sapphire substrate	370, 405, 450 and 520	14, 24, 34, 44, 54, 64, 74, 84 μm		100-435		RZ-OOK	Up to 512 (BER<10^{-10})
2010	[35]	flip-chip AlInGaN μLED on c-plane sapphire substrate	370, 405, 450	72 μm		245 (emission peak=450 nm)		NRZ-OOK	1000 (emission peak=450 nm)

In the column named *diameter*, those filled as A= refer to the active area of those pixels whose shapes are not square or circle.
[a] This cut-off frequency refer to -3dB-electrical frequency f_{-3dB},
[b] This τ is calculated from f_c according to equation $\tau = \sqrt{3}/(2\pi f_c)$
[c] this current density = 6875 A/cm at 110 mW is calculated according to the current density = 375 A/cm at 6mA.

structure (such as the difference in series resistance between top-emitting GaN-on-Si [28] and flip-chip GaN-on -Sapphire [29]). Moreover, the f_c of LED and μLED devices may show dependence on the current density [18], [21], [25], [28] (Table 1) and the temperature [25], [33] (for example, in Tian's work [25]under a current density of 500 A/cm^2, the f_c was around 60 MHz when the device temperature was 425 K while around 80 MHz at 300K).

In conclusion, according to the recent progress, the LED and μLED can reach a f_{-3dB} of more than 1 GHz. The factors that may improve the f_c are: (1) reducing τ_{RC} by reducing the active area A; (2) reducing τ by increasing the overlap between electron and hole wavefunction in spatial integrals in the active layer of the device, such as tuning lattice strain or thickness of the quantum well. Other aspects, such as whether the active layer is grown on c-axial or m-plane, difference in series resistance between top-emitting GaN-on-Si and flip-chip GaN-on-Sapphire, carrier density and temperature, may also influence the f_c.

TABLE 2. Recent progress in color converter materials.

Year	Ref	Material	Form	Light from LED	Φ	τ [ns]	f_c [MHz]	Modulation scheme	Data rate [Mbps]
Organic									
2018	[12]	AIEgens: DM-TPE-BMO	powder	filtered	59%	1.99	128	NRZ-OOK	493
		AIEgens: IQ-TPA	powder	filtered	19%	0.97	279		
2018	[14]	PFBT and PFBT+PF-DBT5 polymer dots	In UV glue NOA60	460 nm LED		1.5	11.1[b]		
2018	[40]	SuperYellow(SY) PPV polymer	on Si-Ag HMMs	filtered		1.71	125	4QAM-OFDM	250
2017	[49]	BBEHBO-PPV	spin-coated film	filtered	45%	0.376	470[a]	NRZ-OOK	>550
2017	[36]	RhB@Al-DBA	MOF	395 nm LED	12%	5.3	3.6[b]	NRZ-OOK	3.6[b]
2015	[2]	BBEHP-PPV + MEH-PPV (90:10)	spin-coated film	filtered	28%	0.278	>200	NRZ-OOK	390
		BBEHP-PPV + MEH-PPV (75:25)	spin-coated film	filtered	25%	0.269	>200	NRZ-OOK	390
2015	[50]	Y-BODIPY	Toluene solution	filtered	62.2%	4.06	39	NRZ-OOK	140
2014	[15]	SY PPV polymer	chlorobenzene solution	450 nm μLED	60%	0.62	>200	DCO-OFDM	1682[c]
Perovskite									
2018	[14]	$CsPb(Br_{0.55}I_{0.45})_3$ QDs	In UV glue NOA60	460 nm LED		19.8	8.2[b]		
2018	[26]	$CsPbBr_{1.8}I_{1.2}$ QDs	epoxy resin (HS-302A) film	filtered	78%	43.7[d]	73	NRZ-OOK	190
2016	[17]	$CsPbBr_3$ NCs + nitride based red phosphor	drop-casted film	450 nm LD	70%	7	491.4[c]	NRZ-OOK	2000[c]
Others									
2019	[51]	CDs from citric acid and b-PEI synthesized via one-step hydrothermal strategy	Drip-coated film	filtered	26%	4	55	NRZ-OOK	181
2019	[10]	CdSe/ZnS QDs	In UV glue	467 nm μLED	90%	17.24	23.1[a]	NRZ-OOK	675[c]
2018	[38]	H_2O_2 treated CDs	doped into the epoxy resin	filtered	25%	6[e]	120	NRZ-OOK	350
2018	[14]	CdSe/ZnS QDs	In UV glue NOA60	460 nm LED	70%	11.2	9.8[b]		
2016	[37]	CdSe/ZnS core/shell QDs	solutions	Blue LED		26.31	2.7[a,b]		
			silicone layer mixed with microsphere	Blue LED			1.90[a,b]		
2016	[52]	$AgInS_2$/ZnS core/shell QDs	in UV glue NOA60	450 nm LED	50%	77	5.4		
2012	[53]	CdSe/ZnS core/shell colloidal QDs	in polyimide matrix	filtered		14	19.7	NRZ-OOK	>25
Phosphorescent materials									
2015	[2]	Phosphors in conventional LED				>50	5		10

The column named *Light from LED* represents the corresponding experimental setup to characterize the color converter. Among these contents, *LED of a certain wavelength* indicates the excitation light source of the color converter that may remain some blue/purple light mixed with the color-converted light, *Filtered* means the light emitted from the blue/purple LED/μLED/LD chip has been filtered by long-pass filter.
The data rates were read from BER-data rate plots where the forward error correction (FEC) limit is $BER=3.8\times10^{-3}$[54], specifically for [2, 50], in which the original author used to estimate data rate from where $BER=1.2\times10^{-3}$.
[a] This cut-off frequency refer to -3dB-electrical frequency f_{-3dB}.
[b] This cut-off frequency may be underestimated due to the limited cut-off frequency of the excitation source.
[c] This cut-off frequency and data rate are overestimated due to the leakage of blue light
[d] The lifetime was characterized in toluene solution, while its f_c and data rate were characterized when it's doped into the epoxy resin
[e] This lifetime was characterized in powder, while its f_c and data rate were characterized when it's doped into the epoxy resin.

2) COLOR CONVERTER

The yellow phosphors used as the color converter in conventional LEDs can only reach a f_c of ∼5 MHz (corresponding to f_{-3dB} of <5 MHz) and a data rate of ∼10 Mbps using non-return-to-zero on-off-keying (NRZ-OOK) [2] (Table 2). Since 2012, researchers have been applying new fluorescent materials to the VLC scenario. These materials can be categorized into organic fluorophores (monomers and polymers) and inorganic ones (perovskite, quantum dots (QDs) and carbon dots (CDs)).

As shown in Table 2, the f_c of the color converter varies in orders of magnitude. Recent research has shown that the f_c of the color converters are inversely proportional to their PL lifetime in the corresponding forms [10], [12], [14]. In order to clarify some confusions in the following discussion, it should be noted that the f_c measured in the literature [17] and data rate in the literature [10], [15], [17] may become larger than the ones predicted by the inversely proportional relation to the PL lifetime τ, due to the influence of blue light. According to the relation between f_c and the power fraction of blue light in white light [10], [14], the f_c becomes close to that of blue LEDs when the power fraction of blue light increases. Some color converters [14], [36], [37] have f_c much smaller than the ones predicted by the inversely proportional relation, which are underestimated by the f_c limit of blue/purple LED to excite the color converter. Moreover, the PL lifetime τ was measured in toluene solution for $CsPbBr_{1.8}I_{1.2}$ QDs [26] and in the form of powder for H_2O_2-treated CDs [38], while their f_c and data rates were characterized when they were doped into epoxy resin. Thus, the τ measurements and communication test (i.e. f_c and data rate) for $CsPbBr_{1.8}I_{1.2}$ QDs [26] and H_2O_2-treated CDs [38] were not in situ.

Generally speaking, the f_c of conventional phosphors, inorganic materials, and organic materials turn out to be in the order of several, tens and hundreds of megahertz respectively. Each type of material has its own advantages and disadvantages. The conventional phosphors have good thermal stability and photostability; however, their f_c can only reach up to a few megahertz. Organic monomers and polymers can reach f_c of hundreds of megahertz, large enough SNR from large enough PL quantum efficiency and varieties of colors to choose from. Nonetheless, some of them have a relatively lower thermal stability and photostability compared with other types of color converter materials. The perovskite and CdSe/ZnS QDs have relatively narrower emission spectrum widths (larger color gamut). However, their f_c are in between the ones of organic fluorophores and conventional phosphors, and the Pb contained in the perovskite and Cd contained in some of the quantum dots are heavy metals with potential health or environmental hazards [39]. Therefore, the choice of color converter materials suitable for VLC usage depends on the application scenario.

Among the organic category in Table 2, the AIEgens refer to a series of luminogens with aggregation-induced emission (AIE) capability (DM-TPE-BMO and IQ-TPA are listed here as examples), RhB@Al-DBA is a dye@metal − organic framework (MOF) hybrid consisting of blue emitting 9,10-dibenzoate anthracene (DBA) linkers and yellow emitting encapsulated Rhodamine B (RhB) molecules, while others are polymers like PPV (SuperYellow is also a kind of PPV), BODIPY and PFBT.

Till the time of writing this article, the BBEHBO-PPV achieved the highest f_c among the novel color converters, whose −3dB-electrical cut-off frequency f_{-3dB} is already ∼470 MHz in spin-coated film (its f_c will be even larger), and other PPV polymers like SuperYellow, BBEHP-PPV and MEH-PPV also have τ of less than 1 ns and f_c of more than hundreds of megahertz. It is surprising to find that SuperYellow exhibits a better f_c and data rate performance in chlorobenzene solution [15] than on Si-Ag hyperbolic metamaterials (HMMs) [40]. However, solution-based color converters are not suitable for mass production as their performances may be influenced by solvent evaporation and leakage.

As for the organic monomers, conventional organic fluorophores like Rhodamine B suffer from aggregation-caused quenching [36], [38], [41], so that their ϕ will reduce when the concentration of the dye molecules increases. One way to overcome this quenching is by using MOF; however, the performance of this MOF hybrid is not fully exhibited due to the f_c limitation of LEDs [36]. Another approach to overcome this quenching is using AIEgens [12], whose f_c can reach up to 279 MHz in the form of powder, and their unique AIE properties that ϕ increases with a rise in concentration will further benefit their usage in solid state lighting.

Among the perovskite category in Table 2, the 8.2 MHz of $CsPb(Br_{0.55}I_{0.45})_3$ QDs [14] may be underestimated due to the limited f_c of the excitation source, and the 491.4 MHz of $CsPbBr_3$ nanocrystals (NCs, which is the same as QDs here) contain the influence of a conventional nitride-based red phosphor and blue laser diode; thus, the 73 MHz of $CsPbBr_{1.8}I_{1.2}$ QDs may be more representative for perovskite QDs. It should be noted that the $CsPbBr_{1.8}I_{1.2}$ QDs exhibit an increase in f_c with a rise in bias current [26].

It should be noted that the absorption and emission of these cesium lead halide ($CsPbBr_{3-x}I_x$) perovskite QDs redshift with an increasing iodide to bromide ratio, which is similar to the phenomena shown in some other perovskite materials in recent publications [42]–[45]. Therefore, it is possible to tune the optical properties of these $CsPbBr_{3-x}I_x$ by anion exchange (changing the value of x) reactions. Compared with the other perovskite used as photovoltaic materials in receivers in Table 3, it can be found that the perovskite materials used as color converters are basically in the forms of cesium lead halide ($CsPbX_3$), while those used as photovoltaic materials are more likely to be in forms of methylammonium lead halide ($MAPbX_3$), where X = Cl, Br, I. This is partially attributed to thermal stability being an important factor for color converters in LEDs [3]. Inorganic cations such as cesium can improve the thermal compositional stability to be thermally stable above 100 $^\circ C$ [46], [47], while organic methylammonium ones may undergo thermal decomposition when the temperature is above 85 $^\circ C$ [48]. According to the absorption and emission spectra of perovskite QDs, changing the cation from methylammonium [6] to cesium [17] causes a blue shift of ∼33 nm. As for the others like CdSe/ZnS QDs, and CDs, it can be found that the reported τ of CdSe/ZnS QDs are around 10-30 ns, and their corresponding f_c are ∼ tens of megahertz if not limited by the blue LED chip [10], [14], [37], [53]. The difference in this τ could be the result of defects [55] and the micro-environmental effect on the PL of these CdSe/ZnS QDs [56].

On the other hand, the f_c of CDs are 55 MHz for those from a one-step hydrothermal strategy using citric acid and b-PEI [51] and 120 MHz for those oxidized by H_2O_2 [38], while their τ are 4 ns and 6 ns respectively. These τ are close to the previously reported lifetime of several nanoseconds of graphene QDs [57], which is promising to achieve a relatively high f_c in QD-like materials. Together with their abundant source, tunable emission and low toxicity [57], [58], CDs can be a competitive candidate for color converter materials together with organic fluorophores like PPV polymers and AIEgens.

It can also be found in Table 2 that besides in forms of powder, spin-coated/drop-casted film, MOF and solution, the color converter dyes also reside in epoxy resin, UV glue, polyimide matrix and silicone. The epoxy resin has advantages of low price and excellent toughness; however, most epoxy resin will yellow over time. The UV glue includes different kinds of materials, for example, the UV glue NOA60 used in [14], [52] is a colorless photopolymer that will cure when exposed to ultraviolet light, so that it does not need to be heated in an oven in its curing operation like

TABLE 3. Recent progress in photodetectors and accessories.

Year	Ref	Material	Responsivity[A/W]	A [mm^2]	Thickness[nm]	Rise/fall time (τ_r) [ns]	f_c [MHz]
Perovskite							
2019	[4]	FTO/TiO_2/ MAPI-1/Spiro-OMeTAD	0.387 (645 nm)	10		183 µs	0.268
		FTO/TiO_2/ FAMA-2/Spiro-OMeTAD	0.372 (670 nm)	10		2.532 µs	0.584
		FTO/TiO_2/ CsFAMA-3/Spiro-OMeTAD	0.349 (665 nm)	10		1.633 µs	0.793
2018	[67]	$CsPbBr_3$+Au/Cr/SiO_2/Si	0.05		16 µm	26/62 ms (τ~15)	
2018	[5]	PTAA,PEIE/$CsPbIBr_2$/PCBM/BCP	0.28 (580 nm)	0.1-7.25	300	20 (0.1 mm^2), 276 (7.25 mm^2)	1.5 (3.625 mm^2), 0.6 (7.25 mm^2)
		PTAA,PEIE/$CsPbBr_3$/PCBM/BCP	0.13 (520 nm)	0.1-7.25	120	62 (0.1 mm^2), 602 (7.25 mm^2)	3 (3.625 mm^2), 1.0 (7.25 mm^2)
2017	[6]	PTAA/$MAPbBr_3$ TSC/C_{60}/BCP	0.26 (540 nm)	0.6-1.5	10 µm	100	4.2
2016	[63]	PTAA/$MAPbI_3$/C_{60}/BCP	0.47 (680 nm)	0.04-7	900-1200	0.95-115.1	
2015	[7]	OTPD/$MAPbI_3$/PCBM/C_{60}	0.21	7.25	400	120	2.9[e]
2015	[45]	Ga/$MAPbBr_3$ SC			1.2 mm	1.56 ms[c]	0.0007
					0.9 mm		0.0016
2014	[8]	PEDOT:PSS/$MAPbI_{3-x}Cl_x$/PCBM		1-10	200-600	180/160	2.9
Silicon							
2019	[69]	MoO_{3-x}/NPPA Si (0.05 Mbps data rate)	0.138 (920 nm)	30	450 µm	0.87 µs/23 µs	0.05
2019	[70]	Si NWs /TiO_2/P3HT	0.59 (920 nm)	70		84 µs /153 µs	
2018	[71]	Ag hyperdoping Si	2.1 (bias = −1V)			12.5 µs /15.9 µs	
2017	[64]	Graphine/Si	0.2	0.0225		2 /5[d]	
2017	[72]	SnTe/Si	2.36	9		2.2 µs /3.8 µs	0.01[f]
2017	[73]	Graphene QD-organic/Si	1.02 (532 nm)			80 µs /70 µs	
2015	[74]	MoO_{3-x}/hierarchical Si	0.056 (920 nm)	9	400 µm	1.03 µs /54.2µs	
		Thorlabs PDA36A (Si PIN)	0.65	13			0.005~10[b]
		Thorlabs PDA10A (Si)	0.44	0.8			150
APD							
		Thorlabs APD430A2 (Si APD)	50 (600 nm)	0.04			400
		Thorlabs APD210 (Si APD)	50 (800 nm)	0.25			5-1000[a]
		Hamamatsu S8664-50K (Si APD)	0.24 (420 nm)	1			60
Accesories							
2016	[68]	Wide FOV fluorescent antenna with a layer of Cm6 in SU-8 coated with epoxy NOA68 (190 Mbps data rate)			~15 µm to PD	τ~3.1	>40

For the content in the column of *thickness* and *rise/fall time* (τ_r), those without extra unit are in the units mentioned in the titles. The parameters for Thorlabs and Hamamatsu instruments are obtained according to the corresponding manuals on its official websites.

For the compound with τ_r of only one value without extra superscript, a short pulse of nitrogen laser light was used to generate carriers in PDs, to capture the transient photocurrent curves. The other rise/fall time with two values separated by a slash were characterized with illumination driven by signal generator of square wave temporal profile.

[a] 3dB-bandwidth in the manual

[b] Depending on the gain, 10 MHz is corresponding to 0 dB setting, while 0.005 MHz (5kHz) is corresponding to 70 dB setting

[c] The device response time was roughly estimated by calculating the electron transit time (t), with the expression of $t=d^2/\mu V$, where d is the crystal thickness (1.2 mm), μ is the electron mobility, and V is the applied bias (−4 V).

[d] Estimated from photocurrent generated from 375 nm pulsed laser.

[e] Calculated from equation $f_{3db} = 0.35/\tau_r$ according to [65] and τ_r.

[f] This cut-off frequency refer to -3dB-electrical frequency f_{-3dB}.

some other UV glue in paper [10]. This NOA60 UV glue is declared to fulfill general adhesive purposes with excellent optical qualities and insulating properties; thus, it can be used as a protective overcoat for color converters on LED devices. The silicone is less rigid than the epoxy and the polyimide, easier to peel off after curing and suitable for bonding large dyes where the stress could cause conformation change in dye molecules [59]. The silicone also has a better heat resistance and yellowing resistance than epoxy resin. The polyimide has higher thermal stability than the epoxy and silicone, which is better suited for application exposed to high temperatures.

It should be noted that some works [60]–[62] have tried to improve the cut-off frequency by filtering out the color-converted light with short-pass(band-pass) filters and selecting only the blue light to generate photocurrent on the receiver. Since the upper bound of the data rate is also influenced by the SNR according to the Shannon-Hartley theorem, if the color-converted light as part of the white light can also be used to generate an effective photocurrent without compromise in cut-off frequency, the VLC system may achieve a larger SNR from a larger photocurrent, and further increase the transmission data rate.

To conclude, according to the recent progress, color converters can reach a f_{-3dB} of up to ~470 MHz for BBEHBO-PPV polymer in spin-coated film, a f_c of 279 MHz for AIEgens monomer in the form of powder, and 120 MHz for H_2O_2-treated CDs which are doped into epoxy resin. Factors that may improve the f_c are: (1) The intrinsic type of color converter material, such as organic fluorophores (monomers and polymers), inorganic ones (perovskite, quantum dots (QDs) and carbon dots (CDs)); (2) The extrinsic form of the material, whether they are in the form of powder, spin-coated/drop-casted film, MOF, solution, UV glue and so forth. Other aspects, such as whether the color converter material has a core/shell structure or not, the micro-environment of the color converter, the bias current of the LED, may also influence the f_c.

B. RECEIVER

For a PD receiver, its cut-off frequency is related to its corresponding response time, and this response time is related to the charge transport and collection property of the active layer, such as charge carrier mobility, thickness and applied electrical bias [8]. The recent rapid development in photovoltaic materials such as perovskite has greatly enlarged the material option for active layer materials that can be used in the receiver of VLC.

According to Table 3, the recent advances in receivers include two categories: one is perovskite PDs and another is silicon-based PDs. Their τ_r can reach as fast as 0.95 ns for perovskite ones [63], and 2 ns/5 ns (rise/fall time) for silicon ones [64]. Among them only part of their modulation frequency response has been characterized and the highest f_c is 4.2 MHz (with a τ_r of 100 ns) for perovskite thin-single-crystal (TSC) PDs fabricated with a vertical P-I-N structure [6], which is comparable to the f_c of commercial PDs such as Thorlabs PDA36A of up to 10 MHz. Since the f_c exhibits inverse proportionality to the τ_r [6], [65], [66], for those PDs with the shortest τ_r of 0.95 ns and 2 ns/5 ns [63], [64], the corresponding f_c can be predicted to be around tens or hundreds of megahertz, which is comparable to commercial PDs like Thorlabs PDA10A and APD430A2.

It can be found in Wu's work [67] that the τ_r of $CsPbBr_3$ when used in PD is 26/62 ms, which is more than 10^6 times larger than its carrier lifetime τ of 15 ns, while the τ of $CsPbBr_3$ NCs as color converter [17] is only 7 ns. It was found that the τ_r measured from a pulsed laser was almost linearly proportional to the A of the device in Shen's work [63], and increased with expanding A (although not linearly proportional) in Bao's work in 2018 [5]. Thus the τ_r of the PD is influenced by the τ_{RC}. On the other hand, it is found in Bao's work in 2017 [6] that the τ_{RC} of those devices were about several nanoseconds (when the capacitance C of those devices were measured to be tens pF, and $R = 50\ \Omega$), and the 100 ns τ_r was dominated by the τ in the perovskite crystal layer. One possibility to resolve these observations is that the τ_r of the device is influenced by two major factors: the τ_{RC} and the τ, in a relation like $\tau_r = \sqrt{\tau_{RC}^2 + \tau^2}$ [10], [65]. The $\tau_{RC} = RC$, where C includes the PD junction and stray capacitance $(C_j + C_s)$. In the PD, the boundaries of the depletion region act as the plates of a paralleled plate capacitor, so that the junction capacitance can be described as $C_j = (\varepsilon\varepsilon_0 A)/W_d$, where ε is the dielectric constant of the photovoltaic layer and W_d is the depletion depth; thus, τ_{RC} will increase with increasing A. Taking Bao's work in 2018 [5] as an example, as A decreases from 7.25 to 0.1 mm^2, the chances are that the τ_r is dominated by τ_{RC} at first since A is relatively large. As A decreases, the τ_{RC} decreases from 276 ns to close to 20 ns, and as A further decreases, $\tau_{RC} < 20$ ns, then the τ becomes dominant in τ_r.

These discussions above indicate that one possible approach to improve the f_c of receivers is via reducing the A of the PD. However, this may reduce the field of view (FOV) of the incoming light collected by the receiver due to the conservation of etendue [68], and thus reduce the SNR. Fortunately, Manousiadis [68] proposed an approach to use fluorescent antenna to exceed this etendue limit, which utilized the fluorescence rather than refraction or reflection of the incoming light to alter the conservation of energy flux to conservation of the number of photons under a certain quantum efficiency. Currently the layer thickness of the fluorescent antenna which can be coupled into the PD is ~15 μm, and the f_c is more than 40 MHz.

As for the photon absorption layers, the perovskite is low-cost and solution-processed with a tunable bandgap; and the silicon is highly reliable with matured manufacturing and a suitable bandgap. Besides, in the literature related to the $MAPbI_3$ [5]–[7], [63], even though the schematic structure of PDs varies, the wavelength ranges of significant responsivity are similar, which cover the range of 350-750 nm, peaking at ~750 nm and then rapidly decrease to longer wavelengths. Thus, it usually uses specific photovoltaic material as the photon absorption layer to achieve a certain range of responsivity. In addition, when the intensity of the incident light increases, the τ_r may also decrease [6].

To sum up, according to the recent progress in PDs, the τ_r can reach as fast as 0.95 ns for perovskite ones, and 2 ns/5 ns (rise/fall time) for silicon ones. Since the f_c is inversely proportional to the τ_r, the corresponding f_c can be predicted to be around tens or hundreds of megahertz. The f_c may be improved by reducing the active area A, and also influenced by the intensity of the incident light. The contraction of field of view when the active area is reduced to enlarge the f_c of PDs can be partially overcome with novel fluorescent antenna, whose f_c is more than 40 MHz. These developments in PDs and accessories are especially promising for VLC scenarios aiming at flexibility or under strong irradiance.

V. INFLUENCE OF THE INCREASE IN THE SYSTEM CUT-OFF FREQUENCY

It has been shown in the previous experimental data and discussion that recent advances in the hardware of VLC can

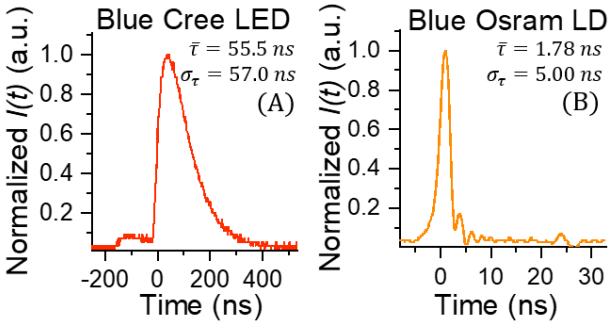

FIGURE 3. The instrument response function of the system with (A) blue Cree LED or (B) blue Osram LD as transmitter and the same APD as receiver. (A) is to exemplify a conventional VLC system before the recent advances in the hardware, while (B) stands for the one after the recent advances.

increase the f_{-3dB} to ∼1 GHz for blue LEDs and 470 MHz for color converters, so that the f_{-3dB} of color-converted light excited by the blue source is calculated to be ∼370 MHz. Compared to the original f_{-3dB} of <5 MHz for conventional white LEDs [2], [12], this increase in $f_{-3dB}(f_c)$ can greatly enlarge the channel capacity of VLC under the same SNR, according to Eq. (1).

On the other hand, the improvement in f_{-3dB} may also improve our understanding of the multipath in the VLC system. To illustrate this claim more clearly, the baseline includes two kinds of temporal profiles, i.e. the instrumental response function (IRF) measured from the real experiment, and the power delay profile (PDP) or channel impulse response (CIR) estimated from the simulation and experiment (the PDP is proportional to the average of square of the CIR over a small local area, as shown in Eq.2 [75]). The effect of the multipath can be investigated from the PDP or CIR. It is known in the optics community that much of the art of temporal profile measurements like PDP, CIR, or carrier lifetime depends on the non-ideal-δ IRF. In the experimental scenario to check IRF, there is a direct irradiation from the light source to photodiode and no reflection from surrounding objects. Hence, to investigate the multipath via PDP (or CIR) of a channel in real scenarios experimentally, it is important to check the corresponding IRF (as shown in Figure 3).

To demonstrate the scenario before the recent advances in hardware, the VLC system is composed of a blue Cree LED as transmitter driven by square pulses (7 ns pulse width and 500 kHz pulse repetition) from the pulse generator (Keysight 81160A Pulse function arbitrary generator of a f_c = 330 MHz), and APD (Thorlabs APD430A2 of a f_c = 400 MHz) as a receiver, its IRF is captured as Figure 3a. On the other hand, to exemplify a system after recent advances, as shown in Figure 3b, a blue Osram LD (PLT5 450B with a f_c of more than 100 MHz) driven by the same pulse generator and received by the same APD is used, since the real system using the novel blue LED, color converter and photodiode will take much more time and effort to build.

To facilitate the comparison between the IRF in a real system before/after the recent advances in the hardware of VLC, as well as the PDP from simulation, here we propose quantities which are named as mean delay $\bar{\tau}$ and root mean square (RMS) delay spread σ_τ, which are defined as follows when the amplitude of the optical signal is $I(t)$ and the power of the optical signal is $P(t)$:

$$P(t) \propto \overline{I^2(t)} \tag{2}$$

$$\bar{\tau} = \frac{\int_0^\infty t \cdot P(t)\, dt}{\int_0^\infty P(t)\, dt} \tag{3}$$

$$\sigma_\tau = \sqrt{\overline{t^2} - \bar{\tau}^2} = \sqrt{\overline{(t-\bar{\tau})^2}} = \sqrt{\frac{\int_0^\infty (t-\bar{\tau})^2 \cdot P(t)\, dt}{\int_0^\infty P(t)\, dt}} \tag{4}$$

where the $\bar{\tau}$ represents the first moment of the power-delay profile with respect to the first delay [77], and the σ_τ can be considered as the measure for delay time extent of a wireless channel. The RMS delay includes the effect of the limited f_c of hardware and multipath spread.

The σ_τ determined from the experiment with a blue Cree LED as the transmitter is around 57 ns. According to Lee's simulation [77], the σ_τ in the scenario of four luminaries being modulated simultaneously at position (1.5, 1.5, 3.0), (1.5, 3.5, 3.0), (3.5, 1.5, 3.0) and (3.5, 3.5, 3.0) and received by the PD at position (0.5, 1.0, 0.0) in a cubic room (5.0 m × 5.0 m × 3.0 m) is about 1.9 ∼ 6.5 ns. When this 57 ns σ_τ of the blue Cree LED system, and the 1.9 ∼ 6.5 ns σ_τ from Lee's simulation are compared, it can be found that the PDP like those in Lee's simulation [77] can be hardly noticed from the real system using a blue Cree LED as the transmitter. This may be one of the reasons that it is mentioned in Pathak's surveys and tutorials in 2015 [78] that most of the current PDPs of VLC depend on simulations, and if we want to get a better understanding of multipath effect in VLC, detailed measurements in real scenarios are essential.

According to Figure 3b, the σ_τ determined from the experiment with a blue Osram LD as the transmitter is 5 ns. which is much smaller than the σ_τ using a blue Cree LED, and comparable in order of magnitude with the 1.9 ∼ 6.5 ns σ_τ from Lee's simulation. Thus, the PDPs related to multipath can be roughly observed from systems like the blue Osram LD system, though its temporal resolution may not be sufficient to resolve the delicate details. To solve this problem, here we propose some directions that may help to characterize the PDP or CIR experimentally: (1) exploration of hardware with a larger f_c than this system with a blue Osram LD and (2) utilization of some ultrafast techniques like femtosecond laser and streak camera.

As the change in channel environment such as furniture in the room may influence the PDP in simulations at the scale of several nanoseconds [79], it can also be derived that the received signal in real experiments will be more susceptible to this change in channel when the f_c of the system increases to hundreds of megahertz. It should also be noted that if the cable length connected to the same signal generator differs by 1.5 m, the delay time generated by the cable will differ

by 5 ns; thus, the cable length is a factor that can influence the synchronization of multiple luminaries and the received signal profile.

VI. CONCLUSION

In this work, the recent developments in the hardware of VLC have been listed and analyzed. Many new materials and devices have been applied to the VLC scenario to test their related performance such as f_c, τ_r and transmission data rates. The f_{-3dB} of blue LEDs, and color converters can reach as high as 1485 MHz and 470 MHz, which are great improvements from the ∼5 MHz f_c of conventional white LEDs. As for the PDs, only a few of the new developed PDs have been characterized directly in f_c, and the largest is 4.2 MHz. Since the smallest τ_r of these PDs is 0.95 ns for $MAPbI_3$ [63], according to the inversely proportional relation between the τ_r and f_c, this $MAPbI_3$ PD [63] is promising to have a f_c of hundreds of megahertz.

Besides, some of the recently developed materials and devices have some unique advantages, such as: (1) the AIEgens [12] as color converters can overcome the aggregation-caused quenching in many of the conventional fluorophores, which are especially useful for scenarios where a high concentration of fluorophore is favored, such as in solid state lighting; (2) by using newly invented fluorescent antenna [68], the decrease in FOV can be partially overcome when a smaller A is used to enlarge f_c.

When the materials and devices are listed and compared between each other, there are some trends extracted from the data: for the electrical-optical LEDs and optical-electrical PDs, (1) as the τ_r is influenced by τ_{RC}, those with a relatively smaller A are more likely to exhibit a smaller τ_r; (2) since the τ_r also includes the carrier lifetime τ, sometimes τ_r can be improved by increasing the overlap between the wavefunction of electrons and holes in the active layer of a device; (3) the f_c may also be affected by the current density for the LED [21] and light intensity for PDs [6].

The enlargement in the f_c of this hardware enables the VLC system to operate at a higher modulation bandwidth without compromise in SNR. This not only enlarges the channel capacity according to the Shannon-Hartley theorem, but also reduces the σ_τ of the IRF of the communication channel. This change in IRF makes it easier to characterize the PDP or CIR of real scenarios experimentally, which can help to improve our understanding of the multipath in VLC. Besides, the VLC system will be more susceptible to changes in the channel, such as the change in furniture [79].

Therefore, the recent advance in the hardware of VLC can not only improve the f_c and transmission data rate, but also facilitate its application to the internet of things.

ACKNOWLEDGEMENTS

The authors would like to thank Rui Wang and Wanli Chen for help with the IRF measurement, as well as Meijuan Jiang, Baikui Li and Sheng Luo for the help to review and make suggestions to this article.

REFERENCES

[1] D. Karunatilaka, F. Zafar, V. Kalavally, and R. Parthiban, "LED based indoor visible light communications: State of the art," *IEEE Commun. Surveys Tuts.*, vol. 17, no. 3, pp. 1649–1678, 3rd Quart., 2015.
[2] M. T. Sajjad, P. P. Manousiadis, H. Chun, D. A. Vithanage, S. Rajbhandari, A. L. Kanibolotsky, G. Faulkner, D. O'Brien, P. J. Skabara, I. D. W. Samuel, and G. A. Turnbull, "Novel fast color-converter for visible light communication using a blend of conjugated polymers," *ACS Photon.*, vol. 2, no. 2, pp. 194–199, 2015.
[3] N. Chi, *Key Devices and Applications of LED Visible Light Communication*. Beijing, China: Post and Telecom Press, 2015.
[4] L. Salamandra, N. Y. Nia, M. Di Natali, C. Fazolo, S. Maiello, L. La Notte, G. Susanna, A. Pizzoleo, F. Matteocci, L. Cinà, L. Mattiello, F. Brunetti, A. Di Carlo, and A. Reale, "Perovskite photo-detectors (PVSK-PDs) for visible light communication," *Organic Electron.*, vol. 69, pp. 220–226, Jun. 2019.
[5] C. Bao, J. Yang, S. Bai, W. Xu, Z. Yan, Q. Xu, J. Liu, W. Zhang, and F. Gao, "High performance and stable all-inorganic metal halide perovskite-based photodetectors for optical communication applications," *Adv. Mater.*, vol. 30, no. 38, 2018, Art. no. 1803422.
[6] C. Bao, Z. Chen, Y. Fang, H. Wei, Y. Deng, X. Xiao, L. Li, and J. Huang, "Low-noise and large-linear-dynamic-range photodetectors based on hybrid-perovskite thin-single-crystals," *Adv. Mater.*, vol. 29, no. 39, 2017, Art. no. 1703209.
[7] Y. Fang and J. Huang, "Resolving weak light of sub-picowatt per square centimeter by hybrid perovskite photodetectors enabled by noise reduction," *Adv. Mater.*, vol. 27, no. 17, pp. 2804–2810, 2015.
[8] L. Dou, Y. Yang, J. You, Z. Hong, W.-H. Chang, G. Li, and Y. Yang, "Solution-processed hybrid perovskite photodetectors with high detectivity," *Nature Commun.*, vol. 5, Nov. 2014, Art. no. 5404.
[9] C. E. Shannon, "Communication in the presence of noise," *Proc. Inst. Radio Eng.*, vol. 37, no. 1, pp. 10–21, Jan. 1949.
[10] H. Cao, S. Lin, Z. Ma, X. Li, J. Li, and L. Zhao, "Color converted white light-emitting diodes with 637.6 MHz modulation bandwidth," *IEEE Electron Device Lett.*, vol. 40, no. 2, pp. 267–270, Feb. 2019.
[11] C. R. Johnson, Jr., W. A. Sethares, and A. G. Klein, *Software Receiver Design: Build Your Own Digital Communication System in Five Easy Steps*. Cambridge, U.K.: Cambridge Univ. Press, 2011.
[12] Y. Zhang, M. Jiang, T. Han, X. Xiao, W. Chen, L. Wang, K. S. Wong, R. Wang, K. Wang, B. Z. Tang, and K. Wu, "Aggregation-induced emission luminogens as color converters for visible-light communication," *ACS Appl. Mater. Interfaces*, vol. 10, no. 40, pp. 34418–34426, Oct. 2018.
[13] M. Rumi and J. W. Perry, "Two-photon absorption: An overview of measurements and principles," *Adv. Opt. Photon.*, vol. 2, no. 4, pp. 451–518, Dec. 2010.
[14] D. Xue, C. Ruan, Y. Zhang, H. Chen, X. Chen, C. Wu, C. Zheng, H. Chen, and W. W. Yu, "Enhanced bandwidth of white light communication using nanomaterial phosphors," *Nanotechnology*, vol. 29, no. 45, Sep. 2018, Art. no. 455708.
[15] H. Chun, P. Manousiadis, S. Rajbhandari, D. A. Vithanage, G. Faulkner, D. Tsonev, J. J. D. McKendry, S. Videv, E. Xie, E. Gu, M. D. Dawson, H. Haas, G. A. Turnbull, I. D. W. Samuel, and D. C. O'Brien, "Visible light communication using a blue GaN μ LED and fluorescent polymer color converter," *IEEE Photon. Technol. Lett.*, vol. 26, no. 20, pp. 2035–2038, Oct. 15, 2014.
[16] A. Rashidi, M. Monavarian, A. Aragon, A. Rishinaramangalam, and D. Feezell, "Nonpolar m-plane InGaN/GaN micro-scale light-emitting diode with 1.5 GHz modulation bandwidth," *IEEE Electron Device Lett.*, vol. 39, no. 4, pp. 520–523, Apr. 2018.
[17] I. Dursun, C. Shen, M. R. Parida, J. Pan, S. P. Sarmah, D. Priante, N. Alyami, J. Liu, M. I. Saidaminov, M. S. Alias, A. L. Abdelhady, T. K. Ng, O. F. Mohammed, B. S. Ooi, and O. M. Bakr, "Perovskite nanocrystals as a color converter for visible light communication," *ACS Photon.*, vol. 3, no. 7, pp. 1150–1156, Jul. 2016.
[18] K. Rajabi, J. Wang, J. Jin, Y. Xing, L. Wang, Y. Han, C. Sun, Z. Hao, Y. Luo, K. Qian, C.-J. Chen, and M.-C. Wu, "Improving modulation bandwidth of C-plane GaN-based light-emitting diodes by an ultra-thin quantum wells design," *Opt. Express*, vol. 26, no. 19, pp. 24985–24991, Sep. 2018.
[19] H. X. Jiang and J. Y. Lin, "Nitride micro-LEDs and beyond—A decade progress review," *Opt. Express*, vol. 21, no. S3, pp. A475–A484, May 2013.
[20] O. Sohail. (2018). *MicroLED vs OLED—Differences, Features, What Can It Change & Everything Else Explained*. [Online]. Available: https://wccftech.com/microled-vs-oled-everything-explained/

[21] S.-C. Zhu, S. Lin, J. Li, Z. Yu, H. Cao, C. Yang, J. Li, and L. Zhao, "Influence of quantum confined Stark effect and carrier localization effect on modulation bandwidth for GaN-based LEDs," *Appl. Phys. Lett.*, vol. 111, no. 17, Oct. 2017, Art. no. 171105.

[22] Y.-F. Yin, W.-Y. Lan, T.-C. Lin, C. Wang, M. Feng, and J.-J. Huang, "High-speed visible light communication using GaN-based light-emitting diodes with photonic crystals," *J. Lightw. Technol.*, vol. 35, no. 2, pp. 258–264, Jan. 15, 2017.

[23] B. Janjua, T. K. Ng, C. Zhao, H. M. Oubei, C. Shen, A. Prabaswara, M. S. Alias, A. A. Alhamoud, A. A. Alatawi, A. M. Albadri, A. Y. Alyamani, M. M. El-Desouki, and B. S. Ooi, "Ultrabroad linewidth orange-emitting nanowires LED for high CRI laser-based white lighting and gigahertz communications," *Opt. Express*, vol. 24, no. 17, pp. 19228–19236, Aug. 2016.

[24] C. Du, X. Huang, C. Jiang, X. Pu, Z. Zhao, L. Jing, W. Hu, and Z. L. Wang, "Tuning carrier lifetime in InGaN/GaN LEDs via strain compensation for high-speed visible light communication," *Sci. Rep.*, vol. 6, Nov. 2016, Art. no. 37132.

[25] P. Tian, J. J. D. McKendry, J. Herrnsdorf, S. Watson, R. Ferreira, I. M. Watson, E. Gu, A. E. Kelly, and M. D. Dawson, "Temperature-dependent efficiency droop of blue InGaN micro-light emitting diodes," *Appl. Phys. Lett.*, vol. 105, no. 17, 2014, Art. no. 171107.

[26] S. Mei, X. Liu, W. Zhang, R. Liu, L. Zheng, R. Guo, and P. Tian, "High-bandwidth white-light system combining a micro-LED with perovskite quantum dots for visible light communication," *ACS Appl. Mater. Inter.*, vol. 10, no. 6, pp. 5641–5648, Feb. 2018.

[27] J.-W. Shi, K.-L. Chi, J.-M. Wun, J. E. Bowers, Y.-H. Shih, and J.-K. Sheu, "III-nitride-based cyan light-emitting diodes with GHz bandwidth for high-speed visible light communication," *IEEE Electron Device Lett.*, vol. 37, no. 7, pp. 894–897, Jul. 2016.

[28] P. Tian, J. J. D. McKendry, Z. Gong, S. Zhang, S. Watson, D. Zhu, I. M. Watson, E. Gu, A. E. Kelly, C. J. Humphreys, and M. D. Dawson, "Characteristics and applications of micro-pixelated GaN-based light emitting diodes on Si substrates," *J. Appl. Phys.*, vol. 115, no. 3, 2014, Art. no. 033112.

[29] J. J. D. McKendry, D. Massoubre, S. Zhang, B. R. Rae, R. P. Green, E. Gu, R. K. Henderson, A. E. Kelly, and M. D. Dawson, "Visible-light communications using a CMOS-controlled micro-light-emitting-diode array," *J. Lightw. Technol.*, vol. 30, no. 1, pp. 61–67, Jan. 1, 2012.

[30] P. A. Haigh, Z. Ghassemlooy, S. Rajbhandari, and I. Papakonstantinou, "Visible light communications using organic light emitting diodes," *IEEE Commun. Mag.*, vol. 51, no. 8, pp. 148–154, Aug. 2013.

[31] I. A. Barlow, T. Kreouzis, and D. G. Lidzey, "High-speed electroluminescence modulation of a conjugated-polymer light emitting diode," *Appl. Phys. Lett.*, vol. 94, no. 24, 2009, Art. no. 243301.

[32] P. Tian, X. Liu, S. Yi, Y. Huang, S. Zhang, X. Zhou, L. Hu, L. Zheng, and R. Liu, "High-speed underwater optical wireless communication using a blue GaN-based micro-LED," *Opt. Express*, vol. 25, no. 2, pp. 1193–1201, Jan. 2017.

[33] M. S. Islim, R. X. Ferreira, X. He, E. Xie, S. Videv, S. Viola, S. Watson, N. Bamiedakis, R. V. Penty, I. H. White, A. E. Kelly, E. Gu, H. Haas, and M. D. Dawson, "Towards 10 Gb/s orthogonal frequency division multiplexing-based visible light communication using a GaN violet micro-LED," *Photon. Res.*, vol. 5, no. 2, pp. A35–A43, Apr. 2017.

[34] R. X. G. Ferreira, E. Xie, J. J. D. McKendry, S. Rajbhandari, H. Chun, G. Faulkner, S. Watson, A. E. Kelly, E. Gu, R. V. Penty, I. H. White, D. C. O'Brien, and M. D. Dawson, "High bandwidth GaN-based micro-LEDs for multi-Gb/s visible light communications," *IEEE Photon. Technol. Lett.*, vol. 28, no. 19, pp. 2023–2026, Oct. 1, 2016.

[35] J. J. D. McKendry, R. P. Greeen, A. E. Kelly, Z. Gong, B. Guilhabert, D. Massoubre, E. Gu, and M. D. Dawson, "High-speed visible light communications using individual pixels in a micro light-emitting diode array," *IEEE Photon. Technol. Lett.*, vol. 22, pp. 1346–1348, Sep. 15, 2010.

[36] Z. Wang, Z. Wang, B. Lin, X. Hu, Y. Wei, C. Zhang, B. An, C. Wang, and O. Lin, "Warm-white-light-emitting diode based on a dye-loaded metal–organic framework for fast white-light communication," *ACS Appl. Mater. Interfaces*, vol. 9, no. 40, pp. 35253–35259, Oct. 2017.

[37] X. Xiao, H. Tang, T. Zhang, W. Chen, W. Chen, D. Wu, R. Wang, and K. Wang, "Improving the modulation bandwidth of LED by CdSe/ZnS quantum dots for visible light communication," *Opt. Express*, vol. 24, no. 19, pp. 21577–21586, Sep. 2016.

[38] Z. Zhou, P. Tian, X. Liu, S. Mei, D. Zhou, D. Li, P. Jing, W. Zhang, R. Guo, S. Qu, and A. L. Rogach, "Hydrogen peroxide-treated carbon dot phosphor with a bathochromic-shifted, aggregation-enhanced emission for light-emitting devices and visible light communication," *Adv. Sci.*, vol. 5, no. 8, 2018, Art. no. 1800369.

[39] A. Babayigit, A. Ethirajan, M. Müller, and B. Conings, "Toxicity of organometal halide perovskite solar cells," *Nature Mater.*, vol. 15, no. 3, pp. 247–251, Mar. 2016.

[40] X. Yang, M. Shi, Y. Yu, Y. Xie, R. Liang, Q. Ou, N. Chi, and S. Zhang, "Enhancing communication bandwidths of organic color converters using nanopatterned hyperbolic metamaterials," *J. Lightw. Technol.*, vol. 36, no. 10, pp. 1862–1867, May 15, 2018.

[41] A. J. Musser, S. K. Rajendran, K. Georgiou, L. Gai, R. T. Grant, Z. Shen, M. Cavazzini, A. Ruseckas, G. A. Turnbull, I. D. W. Samuel, J. Clark, and D. G. Lidzey, "Intermolecular states in organic dye dispersions: Excimers vs. aggregates," *J. Mater. Chem. C*, vol. 5, no. 33, pp. 8380–8389, 2017.

[42] S. Weber, T. Rath, K. Fellner, R. Fischer, R. Resel, B. Kunert, T. Dimopoulos, A. Steinegger, and G. Trimmel, "Influence of the iodide to bromide ratio on crystallographic and optoelectronic properties of rubidium antimony halide perovskites," *ACS Appl. Energy Mater.*, vol. 2, no. 1, pp. 539–547, Jan. 2019.

[43] R. J. Sutton, G. E. Eperon, L. Miranda, E. S. Parrott, B. A. Kamino, J. B. Patel, M. T. Hörantner, M. B. Johnston, A. A. Haghighirad, D. T. Moore, and H. J. Snaith, "Bandgap-tunable cesium lead halide perovskites with high thermal stability for efficient solar cells," *Adv. Energy Mater.*, vol. 6, no. 8, 2016, Art. no. 1502458.

[44] Q. A. Akkerman, V. D'Innocenzo, S. Accornero, A. Scarpellini, A. Petrozza, M. Prato, and L. Manna, "Tuning the optical properties of cesium lead halide perovskite nanocrystals by anion exchange reactions," *J. Amer. Chem. Soc.*, vol. 137, no. 32, pp. 10276–10281, Aug. 2015.

[45] Y. Fang, Q. Dong, Y. Shao, Y. Yuan, and J. Huang, "Highly narrowband perovskite single-crystal photodetectors enabled by surface-charge recombination," *Nature Photon.*, vol. 9, pp. 679–686, Aug. 2015.

[46] J.-W. Lee, D.-H. Kim, H.-S. Kim, S.-W. Seo, S. M. Cho, and N.-G. Park, "Formamidinium and cesium hybridization for photo- and moisture-stable perovskite solar cell," *Adv. Energy Mater.*, vol. 5, no. 20, 2015, Art. no. 1501310.

[47] D. P. McMeekin, G. Sadoughi, W. Rehman, G. E. Eperon, M. Saliba, and M. T. Hörantner, "A mixed-cation lead mixed-halide perovskite absorber for tandem solar cells," *Science*, vol. 351, pp. 151–155, Jan. 2016.

[48] B. Conings, J. Drijkoningen, N. Gauquelin, A. Babayigit, J. D'Haen, L. D'Olieslaeger, A. Ethirajan, J. Verbeeck, J. Manca, E. Mosconi, F. De Angelis, H.-G. Boyen, "Intrinsic thermal instability of methylammonium lead trihalide perovskite," *Adv. Energy Mater.*, vol. 5, no. 15, 2015, Art. no. 1500477.

[49] D. A. Vithanage, A. L. Kanibolotsky, S. Rajbhandari, P. P. Manousiadis, M. T. Sajjad, H. Chun, G. E. Faulkner, D. C. O'Brien, P. J. Skabara, I. D. W. Samuel, and G. A. Turnbull, "Polymer colour converter with very high modulation bandwidth for visible light communications," *J. Mater. Chem. C*, vol. 5, no. 35, pp. 8916–8920, 2017.

[50] M. T. Sajjad, P. P. Manousiadis, C. Orofino, D. Cortizo-Lacalle, A. L. Kanibolotsky, S. Rajbhandari, D. Amarasinghe, H. Chun, G. Faulkner, D. C. O'Brien, P. J. Skabara, G. A. Turnbull, and I. D. W. Samuel, "Fluorescent red-emitting BODIPY oligofluorene star-shaped molecules as a color converter material for visible light communications," *Adv. Opt. Mater.*, vol. 3, no. 4, pp. 536–540, 2015.

[51] E. Liu, D. Li, X. Zhou, G. Zhou, H. Xiao, D. Zhou, P. Tian, R. Guo, and S. Qu, "Highly emissive carbon dots in solid state and their applications in light-emitting devices and visible light communication," *ACS Sustain. Chem. Eng.*, vol. 7, no. 10, pp. 9301–9308, 2019.

[52] C. Ruan, Y. Zhang, M. Lu, C. Ji, C. Sun, X. Chen, H. Chen, V. L. Colvin, and W. W. Yu, "White light-emitting diodes based on $AgInS_2$/ZnS quantum dots with improved bandwidth in visible light communication," *Nanomaterials*, vol. 6, no. 1, p. 13, Jan. 2016.

[53] N. Laurand, B. Guilhabert, J. McKendry, A. E. Kelly, B. Rae, D. Massoubre, Z. Gong, E. Gu, R. Henderson, and M. D. Dawson, "Colloidal quantum dot nanocomposites for visible wavelength conversion of modulated optical signals," *Opt. Mater. Express*, vol. 2, no. 3, pp. 250–260, Mar. 2012.

[54] *Forward Error Correction for High Bit-Rate DWDM Submarine Systems*, document ITU-T Rec. G.975.1, Appendix I.9, 2004.

[55] Y. Kobayashi, T. Nishimura, H. Yamaguchi, and N. Tamai, "Effect of surface defects on Auger recombination in colloidal CdS quantum dots," *J. Phys. Chem. Lett.*, vol. 2, no. 9, pp. 1051–1055, 2011.

[56] Y. Zhang, "Organic fluorophores: Nonlinear optical properties and environmental effects on photoluminescence," Dept. Phys., Hong Kong Univ. Sci. Technol., Hong Kong, Tech. Rep., 2015.

[57] R. Ye, C. Xiang, J. Lin, Z. Peng, K. Huang, Z. Yan, N. P. Cook, E. L. G. Samuel, C.-C. Hwang, G. Ruan, G. Ceriotti, A.-R. O. Raji, A. A. Martí, and J. M. Tour, "Coal as an abundant source of graphene quantum dots," *Nature Commun.*, vol. 4, Dec. 2013, Art. no. 2943.

[58] R. Ye, Z. Peng, A. Metzger, J. Lin, J. A. Mann, K. Huang, C. Xiang, X. Fan, E. L. G. Samuel, L. B. Alemany, A. A. Martí, and J. M. Tour, "Bandgap engineering of coal-derived graphene quantum dots," *ACS Appl. Mater. Interfaces*, vol. 7, no. 12, pp. 7041–7048, 2015.
[59] J. M. Pujol, C. Prud'homme, M. E. Quenneson, and R. Cassat, "Electroconductive adhesives: Comparison of three different polymer matrices. Epoxy, polyimide and silicone," *J. Adhes.*, vol. 27, no. 4, pp. 213–229, 1989.
[60] S.-W. Wang, F. Chen, L. Liang, S. He, Y. Wang, X. Chen, and W. Lu, "A high-performance blue filter for a white-led-based visible light communication system," *IEEE Wireless Commun.*, vol. 22, no. 2, pp. 61–67, Apr. 2015.
[61] J. Armstrong, R. J. Green, and M. D. Higgins, "Comparison of three receiver designs for optical wireless communications using white LEDs," *IEEE Commun. Lett.*, vol. 16, no. 5, pp. 748–751, May 2012.
[62] J. Grubor, S. C. J. Lee, K.-D. Langer, T. Koonen, and J. W. Walewski, "Wireless high-speed data transmission with phosphorescent white-light LEDs," in *Proc. 33rd Eur. Conf. Exhib. Opt. Commun.-Post-Deadline Papers*, Sep. 2007, pp. 1–2.
[63] L. Shen, Y. Fang, D. Wang, Y. Bai, Y. Deng, M. Wang, Y. Lu, and J. Huang, "A self-powered, sub-nanosecond-response solution-processed hybrid perovskite photodetector for time-resolved photoluminescence-lifetime detection," *Adv. Mater.*, vol. 28, no. 48, pp. 10794–10800, 2016.
[64] X. Wan *et al.*, "A self-powered high-performance graphene/silicon ultraviolet photodetector with ultra-shallow junction: Breaking the limit of silicon?" *NPJ 2D Mater. Appl.*, vol. 1, no. 1, Nov. 2017, Art. no. 4.
[65] Optoelectronics OSI. *Photodiode Characteristics and Applications*. [Online]. Available: http://www.osioptoelectronics.com/application-notes/AN-Photodiode-Parameters-Characteristics.pdf
[66] W.-C. Wang, "Optical detectors," Dept. Power Mech. Eng., Nat. Tsing Hua Univ., Hsinchu, Taiwan, Tech. Rep., 2011, vol. 12. [Online]. Available: https://depts.washington.edu/mictech/optics/me557/detector.pdf
[67] Y. Wu, X. Li, Y. Wei, Y. Gu, and H. Zeng, "Perovskite photodetectors with both visible-infrared dual-mode response and super-narrowband characteristics towards photo-communication encryption application," *Nanoscale*, vol. 10, no. 1, pp. 359–365, 2018.
[68] P. P. Manousiadis, S. Rajbhandari, R. Mulyawan, D. A. Vithanage, H. Chun, G. Faulkner, D. C. O'Brien, G. A. Turnbull, S. Collins, and I. D. W. Samuel, "Wide field-of-view fluorescent antenna for visible light communications beyond the étendue limit," *Optica*, vol. 3, no. 7, pp. 702–706, Jul. 2016.
[69] Y. Liu, G. Cen, G. Wang, J. Huang, S. Zhou, J. Zheng, Y. Fu, C. Zhao, and W. Mai, "High performance MoO_{3-x}/Si heterojunction photodetectors with nanoporous pyramid Si arrays for visible light communication application," *J. Mater. Chem. C*, vol. 7, no. 4, pp. 917–925, 2019.
[70] L. Chen, W. Tian, C. Sun, F. Cao, and L. Li, "Structural engineering of Si/TiO_2/P_3HT heterojunction photodetectors for a tunable response range," *ACS Appl. Mater. Interfaces*, vol. 11, no. 3, pp. 3241–3250, Jan. 2019.
[71] X. Qiu, X. Yu, S. Yuan, Y. Gao, X. Liu, Y. Xu, and D. Yang, "Trap assisted bulk silicon photodetector with high photoconductive gain, low noise, and fast response by Ag hyperdoping," *Adv. Opt. Mater.*, vol. 6, no. 3, 2018, Art. no. 1700638.
[72] H. Zhang, B. Man, and Q. Zhang, "Topological crystalline insulator SnTe/Si vertical heterostructure photodetectors for high-performance near-infrared detection," *ACS Appl. Mater. Interfaces*, vol. 9, no. 16, pp. 14067–14077, Apr. 2017.
[73] M.-L. Tsai, D.-S. Tsai, L. Tang, L.-J. Chen, S. P. Lau, and J.-H. He, "Omnidirectional harvesting of weak light using a graphene quantum dot-modified organic/silicon hybrid device," *ACS Nano*, vol. 11, no. 5, pp. 4564–4570, 2017.
[74] C. Zhao, Z. Liang, M. Su, P. Liu, W. Mai, and W. Xie, "Self-powered, high-speed and visible–near infrared response of MoO_{3-x}/n-Si heterojunction photodetector with enhanced performance by interfacial engineering," *ACS Appl. Mater. Interfaces*, vol. 7, no. 46, pp. 25981–25990, 2015/11/25 2015.
[75] T. S. Rappaport, *Wireless Communications: Principles and Practice*. Upper Saddle River, NJ, USA: Prentice-Hall, 2002.
[76] R. K. Saha, "Power Delay profile and channel classification in cellular mobile communications/ a handbook on cellular mobile communication laboratory a MATLAB-based approach," ResearchGate, Berlin, Germany, Tech. Rep. 06, 2016.
[77] K. Lee, H. Park, and J. R. Barry, "Indoor channel characteristics for visible light communications," *IEEE Commun. Lett.*, vol. 15, no. 2, pp. 217–219, Feb. 2011.
[78] P. H. Pathak, X. Feng, P. Hu, and P. Mohapatra, "Visible light communication, networking, and sensing: A survey, potential and challenges," *IEEE Commun. Surveys Tuts.*, vol. 17, no. 4, pp. 2047–2077, 4th Quart., 2015.
[79] M. Uysal, F. Miramirkhani, O. Narmanlioglu, T. Baykas, and E. Panayirci, "IEEE 802.15.7r1 reference channel models for visible light communications," *IEEE Commun. Mag.*, vol. 55, no. 1, pp. 212–217, Jan. 2017.

YILIN ZHANG received the Ph.D. degree in physics from The Hong Kong University of Science and Technology, in 2015, under the supervision of Prof. K. S. Wong. She is currently a Postdoctoral Fellow with the College of Computer Science and Software Engineering, Shenzhen University, China. Her research interests include visible light communication, photophysics, ultrafast spectroscopy, and nonlinear optics.

LU WANG received the B.S. degree in communication engineering from Nankai University, in 2009, and the Ph.D. degree in computer science and engineering from The Hong Kong University of Science and Technology, in 2013. She is currently an Assistant Professor with the College of Computer Science and Software Engineering, Shenzhen University. Her research interests include wireless communications and mobile computing.

KAI WANG received the Ph.D. degree in optical engineering from the Wuhan National Laboratory for Optoelectronics, Huazhong University of Science and Technology, in 2011. He is currently an Associate Professor with the Department of Electrical and Electronic Engineering, Southern University of Science and Technology, China. His research interests include luminescent nanocrystals (e.g., quantum dots and perovskite) and related optoelectronic devices for displays, lighting, and solar energy.

KAM SING WONG received the D.Phil. degree from the Clarendon Laboratory, University of Oxford, in 1987. He is currently a Professor with the Department of Physics, The Hong Kong University of Science and Technology. His research interests include ultrafast laser spectroscopy, nonlinear optical properties of semiconductors and polymers, fabrication and applications of photonic crystals and plasmonic nanostructures, and photophysics of organic and inorganic materials.

KAISHUN WU received the Ph.D. degree in computer science and engineering from HKUST, in 2011. After that, he was a Research Assistant Professor with HKUST. In 2013, he joined SZU as a Distinguished Professor. He has coauthored two books and published over 90 high-quality research papers in international leading journals and premier conferences, such as the IEEE TMC, the IEEE TPDS, the ACM MobiCom, and the IEEE INFOCOM. He is the inventor of six U.S. and over 80 Chinese pending patents. He received the 2012 Hong Kong Young Scientist Award, the 2014 Hong Kong ICT Award for Best Innovation, and the 2014 IEEE ComSoc Asia-Pacific Outstanding Young Researcher Award. He is an IET Fellow.